Chemical State of Nitrogen and Visible Surface and Schottky Barrier Driven Photoactivities of N-Doped TiO2 Thin Films

ARTICLE *in* THE JOURNAL OF PHYSICAL CHEMISTRY C · JULY 2009

Impact Factor: 4.77 · DOI: 10.1021/jp9024816

7 AUTHORS, INCLUDING:

Ana Borras
Spanish National Research Council
64 PUBLICATIONS **722** CITATIONS
SEE PROFILE

Juan Pedro Espinós
Spanish National Research Council
190 PUBLICATIONS **3,436** CITATIONS
SEE PROFILE

José Cotrino
Universidad de Sevilla
110 PUBLICATIONS **1,322** CITATIONS
SEE PROFILE

Agustin R. Gonzalez-Elipe
Spanish National Research Council
434 PUBLICATIONS **7,300** CITATIONS
SEE PROFILE

Chemical State of Nitrogen and Visible Surface and Schottky Barrier Driven Photoactivities of N-Doped TiO_2 Thin Films

P. Romero- Gómez,[†] V. Rico,[†] A. Borrás,[†] A. Barranco,[†] J. P. Espinós,[†] J. Cotrino,[†,‡] and A. R. González-Elipe*,[†]

Instituto de Ciencia de Materiales de Sevilla (CSIC-Univ. Sevilla), Avenida Américo Vespucio 49, 41092 Sevilla, Spain , Departamento de Física Atómica, Molecular y Nuclear. Universidad de Sevilla, Avenida Reina Mercedes 49, 41012 Sevilla, Spain

Received: March 12, 2009; Revised Manuscript Received: May 27, 2009

N-doped TiO_2 thin films have been prepared by plasma enhanced chemical vapor deposition and by physical vapor deposition by adding nitrogen or ammonia to the gas phase. Different sets of N-doped TiO_2 thin films have been obtained by changing the preparation conditions during the deposition. The samples have been characterized by X-ray diffraction, Raman, UV−vis spectroscopy, and X-ray photoemission spectroscopy (XPS). By changing the preparation conditions, different structures, microstructures, and degrees and types of doping have been obtained and some relationships have been established between these film properties and their visible light photoactivity. The N1s XP spectra of the samples are characterized by three main features, one tentatively attributed to Ti−N (i.e., nitride with a binding energy (BE) of 396.1 eV) and two others with BEs of 399.3 and 400.7 eV, tentatively attributed to nitrogen bonded simultaneously to titanium and oxygen atoms (i.e., Ti−N−O like species). By controlling the deposition conditions it is possible to prepare samples with only one of these species as majority component. It has been shown that only the samples with Ti−N−O like species show surface photoactivity being able to change their wetting angle when they are illuminated with visible light. The presence of these species and an additional complex structure formed by a mixture of anatase and rutile phases is an additional condition that is fulfilled by the thin films that also present photocatalytic activity with visible light (i.e., surface and Schottky barrier driven photoactivities). The relationships existing between the reduction state of the samples and the formation of Ti−N or Ti−N−O like species are also discussed.

1. Introduction

The quest for N-doped TiO_2 thin films and powders was fostered by the discovery of Ashahi et al.[1] that titanium dioxide may become photoactive when irradiated with visible light. Since the publication of this seminal work, much effort has been dedicated to both the development of different experimental strategies of doping[2−7] and the understanding of the reasons that make this material photoactive in the visible when appropriately doped.[8,9] However, none of these two questions has yet a clear answer and some controversy exists because the obtained results are not always reproducible. This situation is well reflected in recent reviews dealing with this subject.[10,11]

From an experimental point of view, X-ray photoemission spectroscopy (XPS) has been the most widely used technique to check the state of nitrogen in N-doped TiO_2 materials. Already Ashahi et al.[1] pointed out that there were at least two types of nitrogen species in their N-doped TiO_2. A first one was characterized by a binding energy (BE) of about 396 eV (hereafter called α) and another one by a BE of about 400 eV (hereafter called β). These two species have been determined by XPS with different total and relative intensities in other N-doped TiO_2 materials.[1,6,7,12−16] However, no agreement exists about the assignment of these nitrogen species that have been alternatively attributed to nitride,[1,7,12] NH,[7] molecular nitrogen[7,16] or NO[7,14] species, either in substitutional or interstitial locations of the TiO_2 lattice.

N-doped TiO_2 has been prepared in the form of powder or as thin films. In this latter case, magnetron sputtering,[5,17,18] electron beam evaporation,[19] ion beam-assisted deposition (IBAD),[20] or plasma-enhanced chemical vapor deposition (PECVD)[21] have been utilized. The photoactivity of N-doped TiO_2 thin films can be checked by looking to its photocatalytic ability to produce chemical reactions under the action of light and/or by following the evolution of the wetting angle of water or other liquids on its surface as a function of the irradiation time. As justified in the discussion, we will refer to these two types of photoactivity as "surface" and "Schottky barrier driven" photoactivities, respectively. In some works in the literature, the two effects have been implicitly taken as equivalent. However, this assumption must be considered critically as even for undoped TiO_2 it has been demonstrated that the efficiencies for photocatalytic degradation of dyes and the change in wetting angle upon UV light irradiation can be quite different.[22] In this line, we have recently shown that TiO_2 thin films doped by nitrogen ion beam implantation become partially hydrophilic when irradiated with visible light, even if no photocatalytic activity was observed for these samples.[23]

The present paper addresses some of the aforementioned open issues by studying the synthesis and analyzing the properties of N-doped TiO_2 thin films prepared by PECVD and physical vapor deposition (PVD) at glancing angle evaporation. The plasma and evaporation conditions have been changed to control

* To whom correspondence should be addressed. E-mail: arge@icmse.csic.es.
† Instituto de Ciencia de Materiales de Sevilla (CSIC-Univ. Sevilla).
‡ Universidad de Sevilla.

10.1021/jp9024816 CCC: $40.75
Published on Web 07/07/2009

SCHEME 1: Representation of the Structure of the TTIP and TDEAT Precursors of Ti Used for the PECVD of N-doped TiO_2 Thin Films

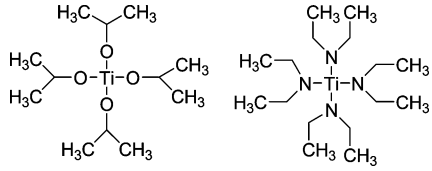

the doping state, the type of species present in the samples, and other properties of the films. In particular, we have tried to correlate the type of species formed in each case with the observed surface and Schottky barrier driven photoactivities of the samples. This latter has been checked by following the photocatalytic degradation of dyes in aqueous solutions. For the purpose of controlling the state and amount of nitrogen into the films, the composition (i.e., nitrogen, oxygen, or hydrogen content) and other characteristics of the plasma used for decomposition of the precursors during PECVD have been systematically changed. In addition, the performance of films from a N-containing precursor (i.e., with Ti−N bonds present in the precursor molecule) is compared with that of films deposited from an standard isopropoxide precursor typically used for the fabrication of TiO_2 optical thin films by PECVD. In this latter case, N-doping of samples is produced by reaction with nitrogen species of the plasma discharge. By PVD, the residual gas during evaporation and the temperature of the substrate have been critical parameters to get thin films with Schottky barrier driven photoactivity in the visible. The films have been characterized by scanning electron microscopy (SEM), X-ray photoemission spectroscopy (XPS), Raman spectroscopy, X-ray diffraction (XRD) and UV−vis absorption spectroscopy. A critical evaluation of the different results obtained has enabled a first assessment of the influence of the state of nitrogen and other thin film characteristics as their structure and microstructure for the visible activation of N-doped TiO_2.

2. Experimental Section

2.1. Thin Film Preparation and Selected Samples. A series of TiO_2 and N-doped TiO_2 thin films were prepared by PECVD in a plasma reactor with a remote configuration. The system, supplied with a microwave plasma source (SLAN, from Plasma Consult, GMBh, Germany) has been described in previous works.[24,25] It consists of an external 2.45 GHz microwave electron cyclotron resonance (MW-ECR) plasma source coupled to the reaction chamber and separated from it by a grid to avoid the microwave heating of the substrates. Under normal conditions of operation, the grid confines the plasma out of the reaction chamber (remote plasma conditions) where the substrate and the precursor dispenser are located. Ion bombardment effects on the growing sample can be enhanced by externally applying a voltage bias to the substrate or by decreasing the operation pressure of the plasma. Control of this effect has demonstrated to be quite effective in modifying the samples characteristics (structure, microstructure), even if the plasma composition remains the same. Titanium tetra-isopropoxide (TTIP) was used as titanium precursor. For comparison, some experiments were also carried out with the nitrogen-containing tetrakis(diethylamido)titanium(IV) (TDEAT) precursor. Scheme 1 shows a representation of the two precursors used in this work. It is worth noting the four direct Ti−N bonds existing in the TDEAT.

The plasma source was operated with a power of 400 W with either pure O_2, O_2 + Ar, or mixtures of gases containing nitrogen, basically $N_2 + O_2$ and $N_2 + H_2 + O_2$. The synthesis of the films was carried out at variable temperatures between room temperature and 523 K, although only results at 298 and 523 K are reported. For dosing TTIP or TDEAT in a controlled way, they were placed in a stainless steel recipient through which oxygen was bubbled while heating at 305 K. Both the bubbling line and the shower-type dispenser used to dose the precursor into the chamber were heated at 373 K to prevent any condensation in the tube walls. Total pressure during deposition was 4×10^{-3} Torr (normal operation conditions). Another series of samples was prepared at a much lower pressure (4×10^{-4} Torr) with $N_2 + O_2$ as plasma gas. In this latter case, the system was working under typical ECR conditions characterized by a higher ion density than at higher pressures.[26] A deposition rate of approximately 2.5 nm min^{-1} was estimated by means of a quartz crystal monitor for the samples grown at room temperature.

Although we prepared a large number of PECVD samples by changing synthesis parameters such as temperature of substrate, pressure, voltage bias applied to the substrate and mixture of plasma gases, we have summarized the results by referring them to the type of nitrogen species detected by XPS. Some basic properties of the set of samples selected for this analysis have been gathered in Table 1, where details about some relevant parameters of the procedure of synthesis are indicated for samples prepared with TTIP as precursor. Occasionally, comments are also made in the text to samples prepared by modifying the preparation parameters reported in Table 1. The order A−E defined in this table has been established after the relative N/Ti ratio determined by XPS as reported in the next section. It can be realized that the thin films were prepared at 298 K (samples C) or 523 K (samples A, B, D, E) by using mixtures of $O_2 + N_2$ that can be rich either in O_2 (samples A) or in N_2 (samples B, C, and E) or also contain H_2 (samples D). A bias voltage of 150 V was applied to the substrate for the majority of the preparations reported in Table 1 (samples B−E). In one case, ECR low-pressure conditions were also used for the deposition of the films (sample E). An undoped TiO_2 sample (sample REF), intended as a reference, was prepared with pure oxygen as plasma gas. A full account of the characteristics of this reference thin film can be found in previous publications.[24,25] From these previous works, an important feature of the undoped TiO_2 thin films prepared by PECVD is that they are amorphous when prepared at $T < 523$ K but become crystalline when prepared at 523 K as temperature of the substrate.

Another series of N-doped TiO_2 thin films were prepared by PVD at glancing angles (i.e., GAPVD).[27−29] The films studied in the present paper were prepared by electron evaporation of TiO_2 as target material and an evaporation angle of 85° between the substrate and the evaporation source. During evaporation, the substrate was kept at 673 K, while a 50% mixture of $NH_3 + O_2$ at a pressure of 10^{-4} torr was dosed in the evaporation chamber. This type of thin films is labeled as sample F. Some of its basic properties are also summarized in Table 1. It is important to indicate that in a similar way than for the PECVD samples other films prepared by PVD using different deposition conditions with nitrogen as the sole residual gas only showed surface photoactivity and will not be considered specifically here.

All the films were deposited simultaneously on a silicon wafer and on quartz plates. Thickness of the prepared samples was estimated by measuring the mass thickness of the films by both

TABLE 1: Summary of Main Properties of Samples

parameter of synthesis				structural and optical properties		
sample	T (K)	plasma composition (N_2%, O_2%, H_2%)	pressure (Torr)	structure[a] and crystal size (nm)	absorption edge	N/Ti
A	523	(17,83,0)	4×10^{-3}	A (84.2)	3.14 eV	0.01
B	523	(88,12,0)	4×10^{-3}	A (85.0)	2.8 eV	0.04
C	298	(88,12,0)	4×10^{-3}	amor	3.32 eV	0.11
D	523	(65,12,23)	4×10^{-3}	amor	2.75 eV	0.11
E	523	(88,12,0)	4×10^{-4}	amor	2.4 eV	0.24
F	673	PVD	10^{-4}	A (22.6) + R (9.0)	2.92 eV	0.01
ref	523	(0,100,0)	4×10^{-3}	A (89.2)	3.22 eV	0

[a] A, anatase; R, rutile; amor, amorphous.

X-ray fluorescence and Rutherford back scattering. Note that the mass thickness is different than the actual thickness of the films determined by scanning electron microscopy and/or by optical methods. Typical (optical) thicknesses of the thin films prepared on silicon or on fused silica substrates were in the order of 300 nm. However, for SEM cross section views, thicker films were prepared on silicon substrates.

2.2. Methods of Characterization. The optical properties of the samples were determined by UV−vis absorption spectroscopy (Perkin-Elmer Lambda 12 Spectrometer) for samples prepared on fused silica. Typical thickness of the samples used for optical characterization was around 350 nm.

XPS spectra of the films were recorded on an ESCALAB 210 spectrometer working under energy transmission constant conditions. The Mg Kα line was used for excitation of the spectra. They were calibrated in BE by referencing to the C1s peak due to contamination taken at 284.6 eV. Quantification was done by calculating the area of the peaks and by correcting then with the sensitivity factor of each element/electronic level. To remove the carbon and other contamination from the surface of the films, they were subjected to a gentle sputtering with Ar^+ ions of 2.5 keV. A current density of about 10 μA cm^{-2} for a sputtering time of 5 min was used in these treatments. Fitting analysis of the N1s peak was carried out by using elemental bands of Gaussian/Lorentzian shape after background subtraction of the spectra with a Shirley-type curve.

SEM cross section and normal images were measured in a Hitachi S5200 field emission microscope for thin films grown on a silicon wafer. The thickness of the samples for SEM analysis was generally higher than for the other characterization experiments.

Structural characterization of the thin films was done by X-ray Diffraction in a Siemens D5000 difractometer.

Raman spectra were collected in a LabRAM HR High Resolution 800 UV Confocal Raman microscope. For the measurements, a green laser (He−Ne 532.14 mn), 600 line/mm, 100× objective, 20 mW, and 100 μ pinhole was used.

Measurement of the surface electrical conductivity of the samples was carried out with the typical four point probe test. A Keithley 617 electrometer and a Hewlett-Packard 34401 A voltammeter were used for the measurements. These consisted of applying a voltage ranging between −0.25 and 0.25 V to the two external probes and the measurement of the current flowing between the two internal probes.

Measurement of contact angle was carried out by the Young method by dosing small droplets of deionized and bidistilled water on the surface of the illuminated samples. In the experiments where the contact angle variation was determined as a function of the illumination time, a metal foil acting as a shutter was used to close and open the lamp output. All wetting angle measurements within a given experiment were taken after illumination for successive periods of time. Therefore, the time scale in the plots refers to the accumulative illumination of the samples. The maximum uncertainty in the determination of the water contact angle is about 10° depending on the sample position. In the course of this investigation, it was noticed that the "as-prepared" thin films were more hydrophilic than the same samples in a given time after their preparation. Therefore, the reported results correspond to samples that were stored in a desiccator, at least for two months, before testing their photoactivity.

Illumination of the samples was carried out with a Xe discharge lamp with a photon intensity at the position of the samples of 2 Wcm^{-2} for the complete spectrum of the lamp. For simplicity we will refer this situation in the text and figures as UV illumination. Other experiments consisted of the illumination with the same lamp by placing an UV filter (i.e., $\lambda = 400$ nm) between the lamp and the sample. The light intensity was then 1.6 Wcm^{-2} at the sample position. In all cases, an infrared filter (i.e., a water bath) was kept between the lamp and the samples to prevent any possible heating by the infrared radiation.

Photocatalytic tests were carried out in a specially constructed experimental setup. It consisted of a small cell made of quartz (total volume 3 cm^3) where 2 cm^3 of a 3.5×10^{-5} M solution of methyl orange dye was placed together with a piece of a silicon substrate (1×0.8 cm^2) with the thin film deposited on its surface. The films, deposited on a silicon wafer, were irradiated from a frontal position while spectra of the solution were simultaneously recorded with the help of two optical fibers connected to an UV−vis spectrometer and placed in opposite sides of the vessel. The solution was bubbled with oxygen and the vessel closed with a Teflon cover to avoid the evaporation of the liquid. The whole setup was refrigerated with a fan placed behind the vessel. This experimental setup permitted the automatic recording of the spectra from the solution while the films are irradiated. Blank experiments were also carried out by placing a piece of a silicon wafer without any TiO_2 thin film deposited on its surface. The intensity of the UV + vis radiation at the position of the cell was 1.8 W (i.e., approximately 0.3 Wcm^{-2} for photons with $\lambda < 380$ nm). Visible illumination was carried out by placing a filter (i.e., $\lambda = 380$ nm) between the Xe discharge lamp and the reaction vessel. The intensity of the visible radiation at the cell position was 160 mW cm^{-2}. Since the illumination area of the samples was defined with a slit of 1 cm^2 and was always the same for all the experiments, their results can be properly compared. The curves reported in the paper to show the evolution of the concentration of dye versus illumination time have been obtained after dividing the curves obtained with the thin films by the curve of the blank experiment. We must stress that placing a silicon wafer in the blank experiment is critical for a proper correction of the results. In fact, in the absence of any reflecting surface in the cell, the

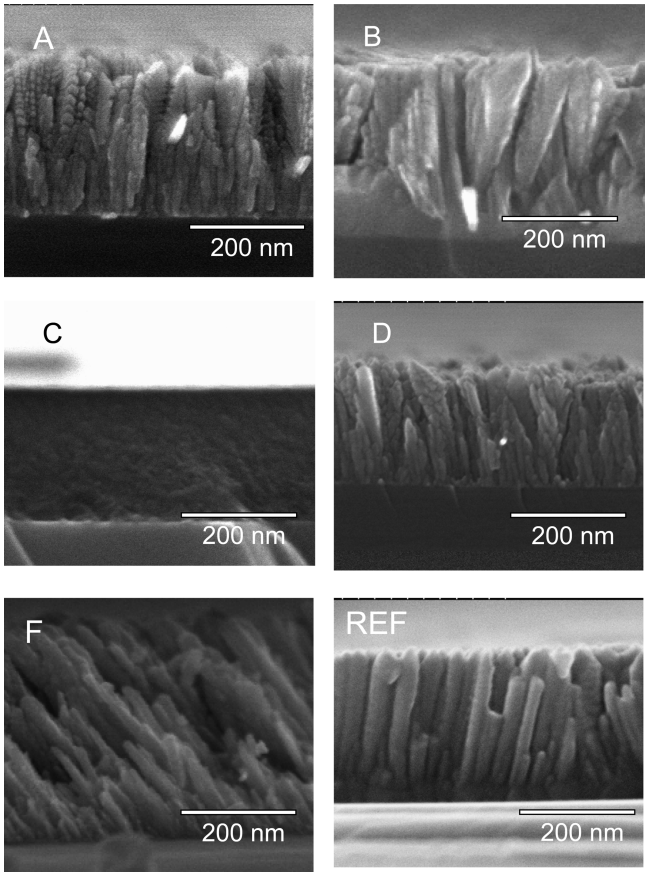

Figure 1. Cross section views of thin films A−F and that of the ref sample. Sample E has a microstructure very similar to that of sample C.

effect of the reflected light through the solution is not considered in the blank experiment and flaw final results are obtained.

3. Results

3.1. Microstructure and Structure of the Thin Films. Figure 1 shows a series of SEM micrographs corresponding to samples A−F and to the reference sample. It is apparent from this figure that the films prepared at 298 K (i.e., sample C) or at 523 K under ECR conditions (i.e., sample E, the image of this latter not shown) present a homogeneous microstructure where no columns or crystals can be seen. A similar microstructure was always obtained under normal pressure conditions of PECVD by applying a high bias voltage to the substrate (i.e., voltages of the order of 300 V, image not shown). This result and the homogeneous microstructure of sample E support that an enhancement of the ion bombardment effects during the film growth favor the surface mobility of the ad-species during growth and, as a result, a homogeneization of the microstructure. This contrasts with the microstructure of the films prepared under "normal" PECVD conditions (i.e., samples A, B, and D) at 523 K as substrate temperature and 150 V as bias voltage, all of them presenting a columnar microstructure formed by the agglomeration of small grains and/or crystallites quite similar to those of the reference sample. The microstructure of sample F prepared by PVD at glancing angles was characterized by tilted columns that leave large open pores between them. This microstructure is typical of this kind of thin films.[29] A rough estimation of the porosity of these films based on the assessment of their refraction indices yields values of the order of 40% of void spaces.

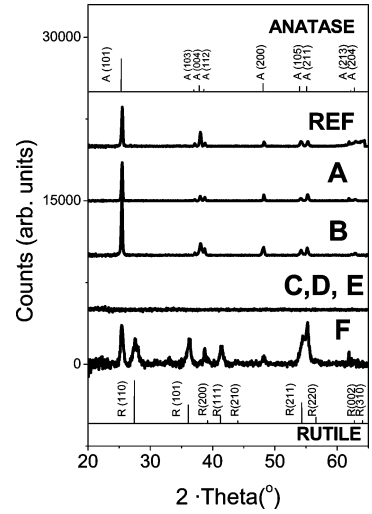

Figure 2. XRD of samples A−F and that of the ref sample included for comparison. Peaks due to the anatase and rutile phases are indicated in the form of patterns.

The structure of the films was analyzed by XRD. The films prepared at 298 K (i.e., samples C) were all amorphous, while those prepared by PECVD at $T > 523$ K (i.e., samples A, B, D and E) were amorphous or crystalline depending on the particular experimental protocol used in each case. Figure 2 reports a series of diffraction diagrams recorded for various samples. The diagrams in this plot corresponding to samples A and B are typical of the anatase structure of TiO_2 although the relative intensity of the different peaks of the diagram slightly differs from that of a polycrystalline sample where the crystals are randomly oriented (see the patterns of anatase an rutile included in the figure for comparison). The crystal size determined by the Scherrer method for the set of samples A and B yielded values of 84.2 and 85.0 nm, respectively. From the (101) peak of the anatase phase of the REF sample, a crystal size of 89.2 nm could be also determined. Samples C, D, and E were amorphous, at least as determined by XRD. This result was quite surprising since samples D and E were prepared by PECVD at 523 K, the temperature at which anatase films are obtained by this method when using an oxygen plasma.[24] Some of these sample characteristics are collected in Table 1. It is also worth noting that a thin film prepared under conditions similar to those of thin films B, but by biasing the substrate with a voltage of 300 V, was also amorphous.

The diagram of samples F prepared by GAPVD, also reported in Figure 2, was characterized by a rich structure where peaks of anatase and rutile can be detected. The crystal size of the anatase phase was estimated in 22.6 nm and that of rutile in 9 nm.

A deeper insight into the structure of the films can be obtained by Raman spectroscopy. Figure 3 (top) shows the Raman spectra of samples A−F compared with the spectrum of the reference sample in the region comprised between 210 and 800 cm^{-1}. These spectra are characterized by a series of peaks with different intensities located at 395, 515, and 638 cm^{-1}.[30,31] Samples C and E have a very poor crystallinity as no resolved peaks of anatase can be detected in this region of the spectra.

The Raman spectrum of samples F shows a more complex pattern where, in agreement with literature,[32] peaks at the positions of the anatase and rutile phases of TiO_2 can be detected. This spectrum confirms the detection by XRD of these two phases.

It is worth stressing that no clear hints of an oxinitride phase could be found in the previous spectra. The formation of this

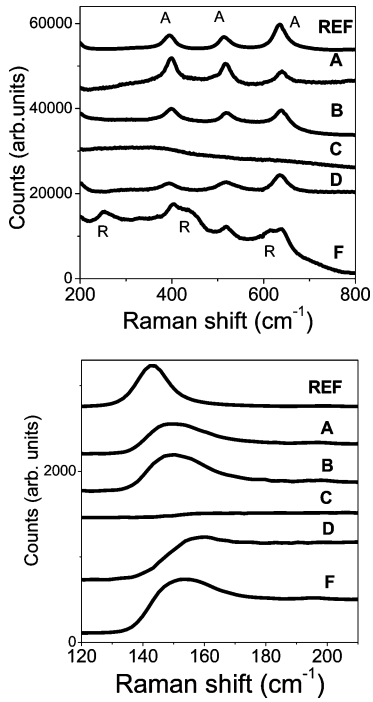

Figure 3. (Top) Raman spectra in the zone between 200 and 800 cm^{-1} for samples A−F compared with that of the reference anatase sample; the peaks attributed to the rutile phase are indicated. (Bottom) Raman spectra in the zone of the main peak of anatase at around 150 cm^{-1}.

phase in N-doped TiO_2 thin films has been claimed by some authors[33] from the fitting analysis of Raman spectra very similar to those of samples A or B in Figure 3. Recently, other authors[34,35] have attributed the background features appearing at around 328, 585, 680, and 815 cm^{-1} to defective titanium oxide. For the case of thin films F, we think that the peaks in Figure 3 (top) around these positions are due to spectral features of the rutile phase detected by XRD.

Figure 3 (bottom) shows an enlarged view around the region of the main peak of the Raman spectrum of anatase attributed to the E_g vibration mode.[30,31] For samples A, B, and F and even more pronounced for sample D, the position of the main mode at around 150 cm^{-1} is shifted from 143.2 cm^{-1} in the reference anatase to around 150.0 cm^{-1} and beyond in samples A, B, F, and D. In these four cases, the peak also broadens with respect to the peak of the reference sample. It is important to remark that for sample D no well-resolved diffraction peaks could be observed by XRD, thus sustaining that Raman can be a more sensitive technique to detect first crystallization stages in thin films. Frequency shift and line width broadening of the main mode have been attributed to crystalline size effects[33−35] and/or to the accumulation of structural defects and/or lack of stoichiometry of the oxide.[36] Since the crystal size determined by XRD is not much smaller in samples A and B (although it is smaller in sample and F) than in sample REF, we must conclude that accumulation of structural defects and/or some chemical reduction with a loose of stoichiometry are likely the main reasons for the observed Raman shift in these samples.

3.2. UV−vis Spectra and Reduction Degree of the Films. A first assessment of the reduction state of the oxide thin films was obtained by measuring their surface conductivity. Samples A, B, C, and F present a high surface resistivity and no reliable final data on sheet resistance could be obtained with the used technique. However, surface conductivity in the dark could be measured for samples D and E. Sample E was the most conductive one with an estimated resistivity of 1.5×10^{-1} (cm Ω). The measured values were dependent on the time elapsed since the preparation of the samples with the conductivity slightly decreasing for the sample stored for long periods of time. Surface conductivity in titanium oxide thin films is associated with the presence of vacancies and other structural defects within a layer of several tenths of a nanometer, indicating a certain lost of stoichiometry (i.e., formation of Ti^{3+} species).[37,38]

Figure 4 shows the UV−vis absorption spectra of samples A−F, together with the spectrum of the anatase thin film taken as a reference. The value of the absorption edges, obtained by the Tauc method by extrapolating to zero the function $A(h\nu)^{1/2}$,[39] is reported in Table 1. The obtained data indicate that samples A and C present absorption edges that are very close to that of the reference anatase film, while samples B, D, E, and F present absorption edges that are shifted to smaller energies. In addition, samples B, D, E, and F present some specific absorption features in the blue region of the spectra that are clearly distinguishable from the typical interference oscillations presented by high refraction index thin films deposited on a quartz substrate. For samples B, D, and F, this first absorption feature is located around 420 nm. In samples E, besides an absorption around this wavelength, there is also a broad absorption extending through the whole range of wavelengths and centered at $\lambda = 500$ nm. Very likely this broad absorption is related with the existence of a high concentration of structural defects and/or Ti^{3+} species as it can be deduced from the relatively high surface conductivity of this sample.

The absorption spectra of N-doped titanium oxide has conceited much interest in literature because absorption features in the visible have been taken as a hint of visible photoactivity of this material and because of a vivid controversy about the effect of doping in narrowing the band gap of TiO_2.[10,11] According to Serpone et al.[40] absorption features appearing in the visible in anion-doped titanium oxide originate from color centers associated with the reduction of the titanium oxide rather than with a narrowing of the band gap as claimed by others.[41−43] Meanwhile, Lin et al.,[44] combining theoretical calculations with the analysis of UV−visible spectra, concluded that the optical absorption of N-doped TiO_2 is primarily located between 400 and 500 nm, while that of oxygen-deficient TiO_2 appears above 500 nm. These authors coincide in that no narrowing of the band gap of TiO_2 occurs as an effect of the incorporation of nitrogen into the structure of the oxide. In relation with our results, we can tentatively assume that samples E, depicting a broad absorption at $\lambda = 500$ nm and showing a measurable surface conductivity, is chemically reduced and presents a considerable concentration of oxygen vacancies and other defects in its structure. Meanwhile, the absorption features at around 430 nm found in samples B, D, and F are likely related with absorption centers associated to nitrogen incorporated within the structure of the titanium oxide.

3.3. XPS Analysis and Chemical State of Nitrogen. XPS has been used to check whether nitrogen has been incorporated within the structure of the titatium oxide films. This technique also provides information about the actual chemical state of nitrogen in the different samples. Figure 5 shows N1s fitted photoemission spectra recorded for samples A−F. The spectra are represented by applying different multiplication factors to bring all the spectra to a similar height. The N/Ti ratios determined for these samples are reported in Table 1. The obtained data show that samples C, D, and E have a high content of N, while in samples A and B this amount approximately decreases by one order of magnitude. Sample F presents a spectrum that is similar to that of sample A. To a first

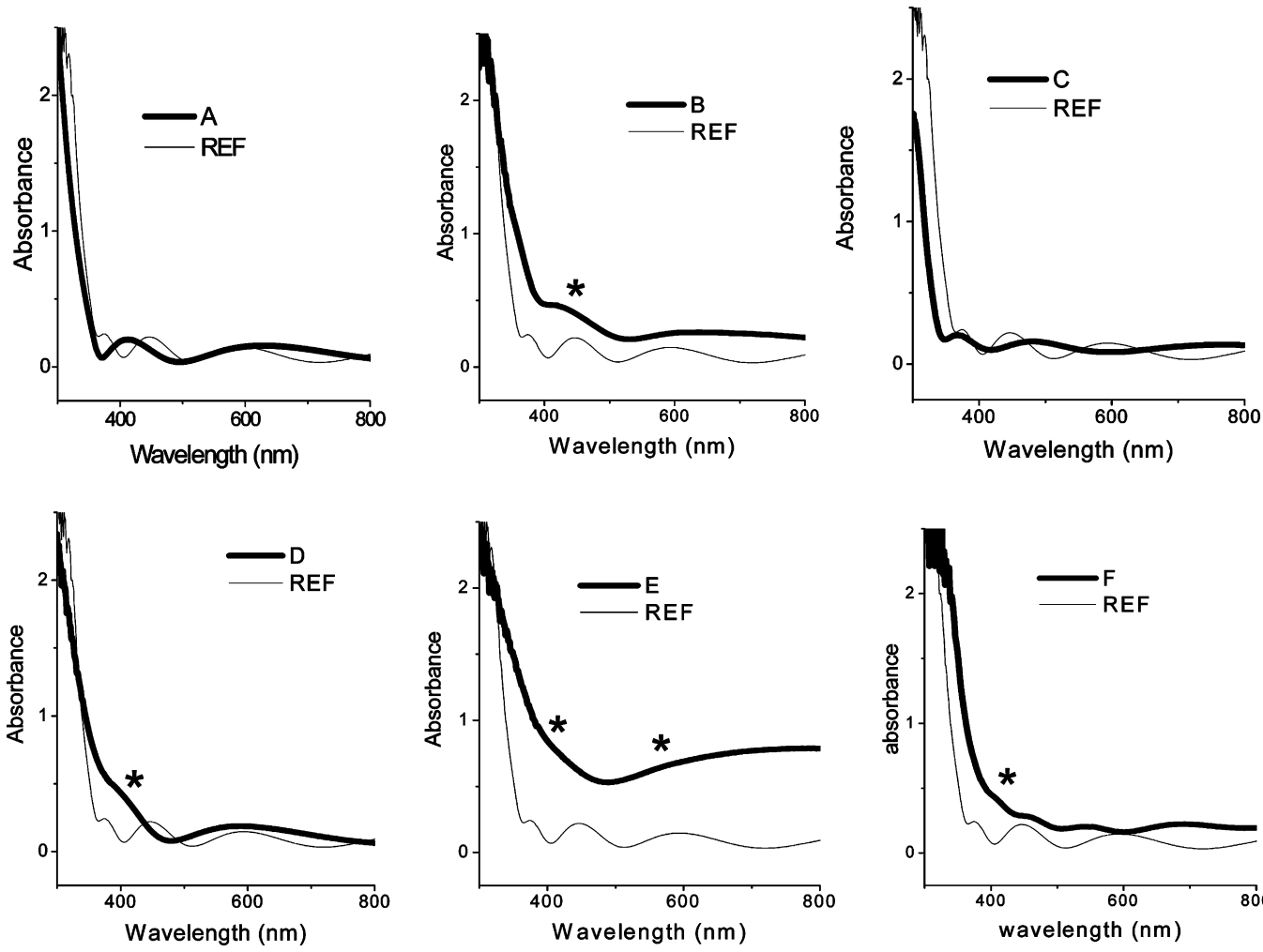

Figure 4. UV−vis absorption spectra of samples A−F compared with that of the reference thin film. The asterisk in some of the plots indicates the presence of a specific absorption feature.

approximation, the N1s spectra in Figure 6 can be considered as the contribution of three main components, a first one centered around 396 eV (species α) and two others centered around 400 eV (species β and β'). Photoemission spectra of the O1s, C1s, and Ti2p levels were also recorded. The O1s and Ti2p spectral shapes were quite similar in all cases and equivalent to the reported spectra of TiO_2 (i.e., attributed to $O^=$ and Ti^{4+} species[45]). The corresponding spectra are reported in the Supporting Information S1. The C1s spectra was characterized by a main peak at 284.6 eV, taken as a reference for the BE scale. In some cases a small shoulder at about 290 eV could be observed in the spectra. This peak is normally attributed to carbonate species,[46] while the main peak is ascribed to carbonaceous rests contaminating the surface of the samples. For the PECVD samples, another source of this spurious carbon can be some adsorbed rests of the organic parts of the titanium precursor. The amount of contaminating carbon (i.e., around 15% atomic) was similar to that detected in other oxide thin films handled in air. Its surface character was confirmed by subjecting the examined thin films to a mild sputtering treatment for 5 min (see Experimental Section). After this treatment, the carbon content in the samples decreased to less than 7% atomic in all cases. This contrasts with the fact that the N/Ti ratios measured for the sputtered films remained almost unmodified after that treatment. This supports that nitrogen is distributed homogenously through all the films. Apart from a broadening in the spectral shape, the form of the N1s spectra in the different samples was not modified significantly after that treatment (see Supporting Information S1). This indicates that the different species identified in the spectra of Figure 5 distribute homogeneously through the first layers of the films. It is also interesting that in sample E subjected to the sputtering treatment, the Ti2p level depicted a shoulder at 456.5 eV that can be attributed to Ti^{3+} species. In the other samples, such a feature is not so clearly observed (note that TiO_2 is always reduced when subjected to Ar^+ sputtering due to the preferential loss of oxygen[47]). This result sustains the previous evidence in Section 3.2 in the sense that this sample is partially reduced.

In relation with the XPS analysis of samples, it is also important to remark that, particularly for samples D and E and to lesser extent B, the spectra underwent a certain evolution with time. This evolution is characterized by a relative decrease in the α band at 396 eV and an increase in the intensity of the β bands around 400 eV.

A deeper insight into the type of nitrogen species that become incorporated into samples A−F can be obtained by the fitting analysis of the spectra in Figure 5. We have intended such an analysis under the assumption that all the spectral shapes can be well reproduced by the contribution of three bands centered at 396.1 (species α), 399.3 (species β), and 400.7 (species β') eV. The results of the fitting analysis are reported in Figure 5. The fitting scheme used implies that around 396 eV there is only one type of nitrogen species, while around 400 eV there is the contribution of two different bands. It is important to note

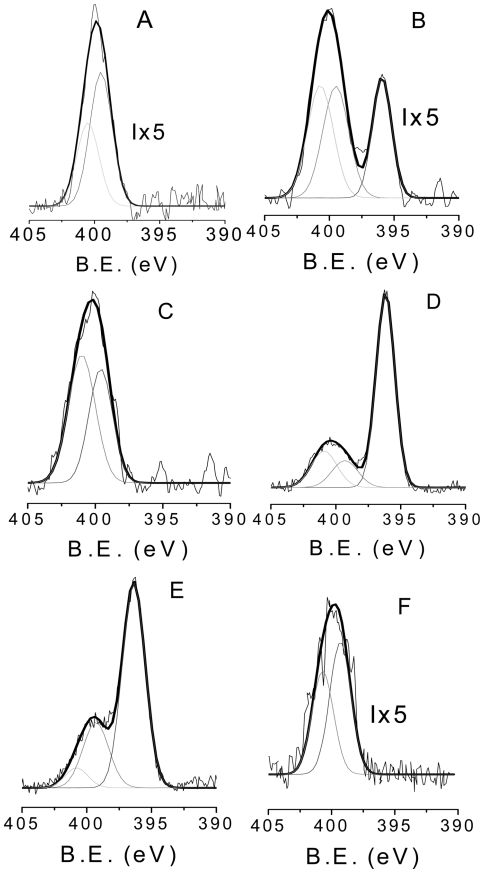

Figure 5. N1s fitted photoemission spectra of samples A−.F.

that this fitting scheme based on the presence of three bands provides the minimum number of fitting bands with a similar width (i.e., between 1.7 and 1.4 eV) that would be common for the six analyzed spectra. However, we must stress that this analysis does not discard the presence of other possible species characterized by BEs similar to those of the three bands resulting from the fitting analysis.

The XPS analysis of the state of nitrogen in N-doped TiO_2 thin films has been widely addressed in the recent literature on the subject,[1,8,10−16,33,48−51] although no agreement exists neither about the attribution of the detected species nor about the species which is/are responsible for the visible light photoactivity of N-doped TiO_2. Of particular interest is the recent paper by Asahi et al.[51] who based on first-principles calculations using the projector argument wave method[52] has attributed the observed peaks in a series of N-doped TiO_2 photocatalysts to N (395.7 eV), NO (398.1 eV), and NO_2 (399.8 eV) species. Nitrogen species with BEs around these values have been detected during the oxidation of titanium nitride compounds[53,54] or by the nitrogen implantation in titanium and other metal oxides.[55,56] On the basis of these previous works, we tentatively ascribed the species detected in our films to nitride (396.3 eV) (i.e., nitrogen triple bonded to titanium) and to nitrogen in a titanium oxinitride local environment (399.3 and 400.7 eV) where nitrogen simultaneously bonds to oxygen and to titanium in a defective lattice site (i.e., in a kind of Ti−N−O local structure). Within this scheme, a different covalent character of the N−Ti bond would account for the differences in BE between the two β species (e.g., structures of the type Ti−N−O···Ti or Ti−O−N···Ti). Basically, this tentative attribution assumes some kind of bonding between nitrogen and oxygen for the species yielding the peaks at around 400 eV. In line with some previous reports on this subject,[11] the latter attribution assumes that the nitrogen is also bonded to titanium. On the other hand, the need of bonding to an electrophilic atom is a requirement because species like NO^-, NO_2^-, or NO_3^- where nitrogen is solely bonded to oxygen atoms are characterized by BEs larger than 402 eV[57] and molecular nitrogen species implanted in oxides are characterized by a BE of 403.4 eV.[56] In our case, the attribution of the nitrogen species at around 400 eV to a nitrogen atom simultaneously bonded to oxygen and titanium of the lattice was further sustained by the analysis of a N-doped TiO_2 sample prepared by PECVD using TDEAT as precursor and a plasma of pure oxygen. In that case, only a N1s broadband at around 400 eV with a N/Ti ratio of 0.01 could be detected even if no nitrogen was present in the plasma (see Supporting Information S2). The fact that in the TDEAT precursor there are four nitrogen atoms directly bonded to the titanium supports that after extensive oxidation of the precursor during the plasma deposition process, some nitrogen may remain directly bonded to the Ti although also interacting with the oxide ions of the lattice.

3.4. Photoactivity of N-doped Thin Films. A first way of probing the photoactivity of titanium oxide thin films is by measuring the wetting contact angle for samples exposed to illumination with UV, vis, and/or UV + vis light. As indicated in the Introduction, we will refer to this experiment as surface photoactivity. Another way is by measuring the photocatalytic activity of the films.[58−61] These experiments will be denoted here as Schottky barrier driven photoactivity. In a recent publication on undoped TiO_2,[22] we have pointed out that these two tests are not equivalent and that they may yield different information about the photoactivity of the studied systems. Here, we have tested the surface photoactivity of the different films by measuring the evolution of the wetting angle when they are illuminated with vis and UV + vis lights as a function of the irradiation time. Schottky barrier driven photoactivity tests consist of measuring the photocatalytic degradation of methyl orange dye in an aqueous solution.

Figure 6 shows four experiments taken as examples of the surface photoactivity behavior of the different thin films when they are illuminated, first with visible light and then with UV light. The recovery of the wetting angle in the dark is also included. The behavior depicted by the REF thin film and sample E is typical of stoichiometric TiO_2 surfaces and consists of the transformation of the surface of this material from hydrophobic into superhydrophilic when illuminated with UV light.[62] When the film is left in the dark, it slowly recovers the initial wetting angle. These processes are affected by the topography of the surfaces and large variation in wetting angles can be produced for nanostructured thin films in the form of fibers or similar nanostructures.[63] In our case, a similar behavior was also observed for samples C and D. The plots on the right side of Figure 7 depict the behavior of samples A and F. Sample B also follows a similar pattern. These plots are characterized by a partial and slow decrease in wetting angle for about 30−40 °C when these thin films are illuminated with visible light and a subsequent sharp decrease when the films are illuminated with UV + vis light. In the dark, the films slightly recover the wetting angle reached upon visible light illumination. A similar behavior has been previously reported by us for N-doped TiO_2 and Ta_2O_5 thin films prepared by ion implantation[23,29] or by other authors for thin films prepared by magnetron sputtering.[64] In other works from literature, complete transformation into the superhydrophilic state of the surface of N-doped TiO_2 thin films upon visible light irradiation has been also reported.[65]

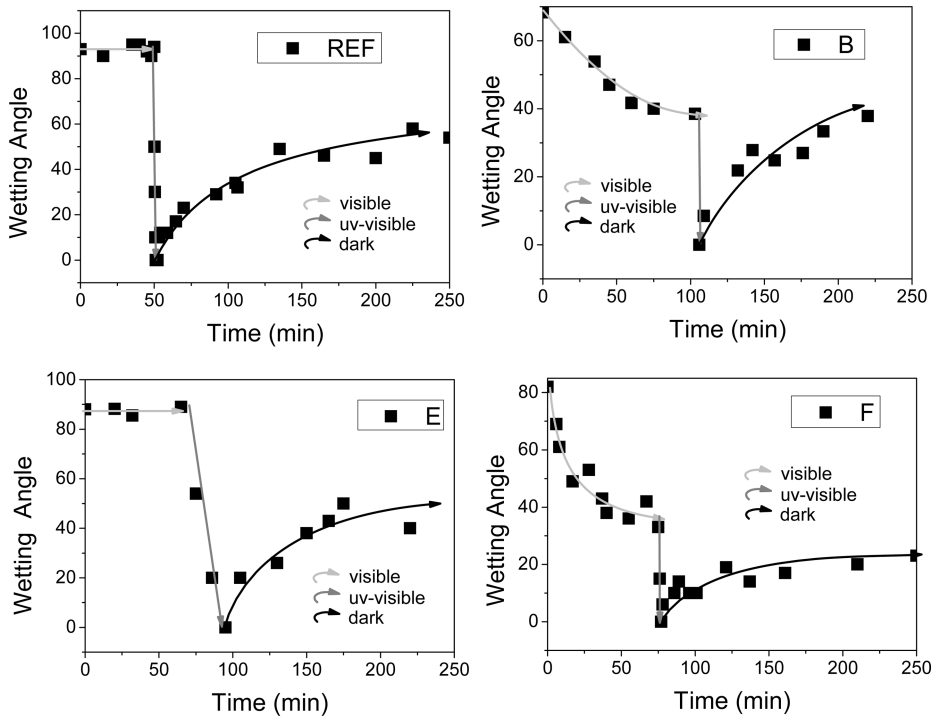

Figure 6. Evolution of the wetting angle for the REF and E thin films (left) and samples A and F (right) subjected sequentially to illumination with visible, UV + vis, and then left in the dark. The curves are plotted to guide the eyes.

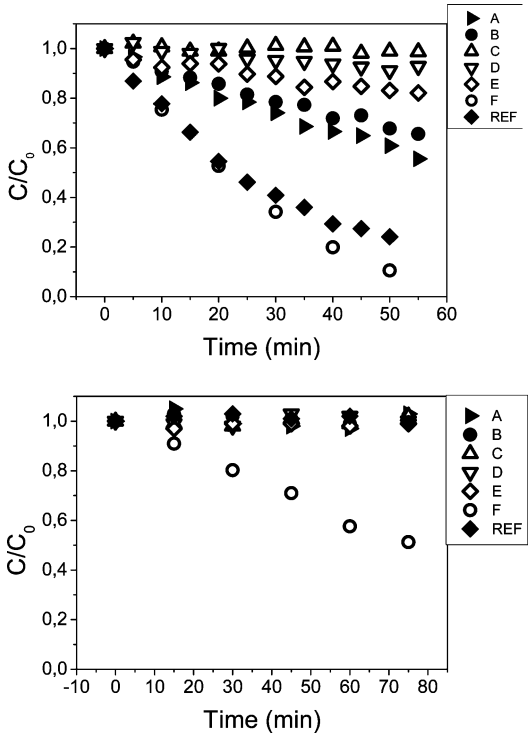

Figure 7. Evolution of the concentration of methyl orange dye in an illuminated solution of this molecule in the presence of the thin films. Curves corresponding to experiments with UV + vis (top) and vis (bottom) illumination are reported. The curves upon UV + vis illumination have been corrected by the curve of a solution of the dye in the presence of a bare sustrate of Si without thin film.

The Schottky barrier driven photoactivity of films A−F toward the degradation of the methyl orange dye was analyzed by illuminating with visible and with visible + UV light. We observed that none of A−E films presented a detectable activity in the visible, while samples A and B were active for photodegradation of the dye only when they were illuminated with UV + vis light; however, this activity was smaller than that of the reference sample. Meanwhile, thin films F were active with both visible and UV irradiation. A comparison of the activity of the different films is reported in Figure 7 for illumination with UV + vis and vis lights. The lack of Schottky barrier driven photoactivity in the visible for samples A−E is somehow contradictory with previous works in literature reporting the visible photodegradation of dye solutions with N-doped TiO_2 materials.[1,8,33,51,57−61] Differences in experimental conditions, such as the use of methylene blue (MB) as sacrificial dye in most of these previous works or the fact that we are working with nanometric thin films and not with powders might be reasons for this discrepancy. In fact, while the methyl orange solutions used in our case are stable under visible light irradiation (but not under UV irradiation), MB solutions are not stable either under UV or visible illumination. According to our experience, this and other factors generally not considered explicitly in the experimental parts of the papers, such as the control of both the concentration of oxygen and the temperature in the reaction vessel during illumination or the inner vessel reflectivity in the blank experiments are factors that, if not properly handled, may lead to flaw experiments and misleading results (e.g., uncontrolled direct light degradation of the dye in the solution).

4. Discussion

The analysis of samples A−F has shown that they present different structures, microstructures, and compositions. XRD and Raman analysis of samples (cf. Figures 2 and 3) have shown that only samples A and B present well-defined peaks attributed to the anatase structure. According to the Raman spectra in Figure 3, samples D also present an incipient crystallinity. Meanwhile, F samples consist of a mixture of the anatase and rutile structures of TiO_2. The poor crystallinity of samples D must be related with the enhancement of ion bombardment effects during the preparation of the samples under ECR

conditions.[24,25] Meanwhile, the amorphous character of samples E, even if prepared at 523 K by PECVD, is likely related with the considerable reduction degree of these samples and/or with the high concentration of Ti−N species incorporated into their structure. On the other hand, comparison of the main peak of the Raman spectra of the reference sample and those of samples A, B, and F indicates that these N-doped thin films present a considerable concentration of structural defects. We think that the incorporation of nitrogen within the structure of these samples is contributing to this effect.

The amount and chemical character of nitrogen incorporated in the structure of the films was also different depending on the sample. The concentration of nitrogen follows the order E > D = C > B > A = F (cf. Table 1), a similar trend than for the ratio $\alpha/(\beta + \beta')$ between the different kinds of nitrogen species. It is important to remark that samples E, characterized by the highest absolute and relative concentrations of both nitrogen and species α, respectively, present a high reduction degree. This result proves the existence of a link between the formation of Ti−N species of the α type and the reduction degree of titanium oxide.

Species $\beta + \beta'$ are the majority in samples A, B, and F with all of them prepared under mild oxidant conditions and, consequently, with little or no lattice reduction. Quite interesting is that only these samples present surface photoactivity in the visible. According to our tests, this means that species α with a BE around 396 eV (attributed to Ti−N) would be inactive for the visible photoactivation of N-doped TiO_2 and that the presence of species β and/or β' is a requirement for surface photoactivity in the visible. Some hints in the recent literature on the subject[12,33,50] agree with this behavior of samples A−F. This finding is in apparent contradiction with previous reports in literature where the photoactivity of N-doped TiO_2 thin films has been associated with the presence of species α,[1,64] although in most cases the two species, α and β, have been simultaneously detected. Without discarding other effects, a possibility is that in many previous experiments dealing with N-doped TiO_2 samples the distribution of nitrogen species is heterogeneous, so that the measured photoactivity in the visible responds exclusively to those parts of the samples with a majority concentration of $\beta-\beta'$ species. In powder materials, this heterogeneity might correspond to a different distribution of nitrogen species in the individual grains of the specimens. In thin films inhomogeneities in the depth distribution of nitrogen species might be an additional factor modifying the visible photoactivity of samples.

It has been generally considered that visible photoactivity of N-doped TiO_2 is linked with a shift in the position of the absorption edge.[10,11] Without completely contradicting this view, our results with samples A−F introduce some nuances that deserve a specific consideration. Data in Table 1 suggest a certain correlation between the concentration of nitrogen in the sample and the magnitude of the shift in the absorption edge. This means that those samples with a high concentration of the α species present a maximum shift in the absorption edge. This finding precludes an automatic use of the value of the absorption edge as a measurement of photoactivity since we have demonstrated that this species does not contribute to the visible photoactivity of the system. In this regard, it is worth noting that samples A, even presenting surface photoactivity in the visible attributed to the incorporation of species β/β' in its structure (cf. Figure 5), do not present any significant shift of the absorption edge. This suggests that other factors like lattice reduction or the presence of other defective sites associated to nitrogen must contribute to the shift in the absorption edge. A similar description has been proposed by Serpone et al.[11,40] to account for the edge shift in N-doped TiO_2.

From the three samples, A, B, and F, that present surface photoactivity in the visible, only sample F presents Schottky barrier driven photoactivity. From the point of view of XPS, this sample is very similar to sample A, although structurally sample F consists of a mixture of anatase and rutile and presents a shifted edge and some absorption band in the visible (cf. Table 1). This result suggests that the development of local electronic heterojunctions between zones consisting of N-doped anatase and N-doped rutile could be a condition for the Schottky barrier driven photoactivity of this type of samples. It could be also possible that in these samples, a minority oxinitride phase not detected in the Raman spectrum is responsible for the observed photocatalytic activity. At present, more experimental and theoretical work is being carried out to ascertain these hypotheses.

In any case, the photoactivity results found for samples A, B, and F permits one to establish that wetting angle variation and photocatalytic activity are two related but different manifestations of the photoactivity of N-doped TiO_2. The terms surface and Schottky barrier driven photoactivities used for convenience through all this manuscript deserve now a justification. Photocatalytic degradation of dye molecules is a complex process implying the migration of photoexcited electrons and holes from the irradiated solid up to its surface. The migration of UV-induced photoholes through the valence band of TiO_2 is the rate controlling step of this process and is driven by the formation of a Schottky barrier at the surface.[10,11,66] A similar migration of photoholes produced by visible light should be expected in the case of N-doped TiO_2. However, such a migration from the bulk would only be possible is the electronic states associated to nitrogen form a continuous band (or interband located between the valence and conduction band of TiO_2[8,9]). Although we have to explore further the reasons why samples F present Schottky barrier driven photoactivity, it is reasonable to think that the formation of anatase/rutile heterojunctions could contribute to favor the migration of photoholes from the interior of the material up to its surface. In this regard, it is worthy of mention a recent paper by Zhang et al.,[67] showing that in TiO_2 powders, consisting of rutile grains covered by small anatase nanoparticles, the photocatalytic reduction of ethanol or water toward the formation of H_2 is enhanced with regard to a sample consisting of pure anatase.

On the other hand, surface photoactivity, manifested as a change in the wetting angle by visible irradiation of the N-TiO_2 thin films, would be a less strict process if just the photoholes generated at the outmost surface layer(s) intervene in the photoinduced reaction. Since the number of photoholes required to induce the change in wetting angle is expected to be much smaller than for a sustained photocatalytic process, it is reasonable to assume that just photoexcitation processes affecting the topmost layer of the sample may be enough to modify this surface property. Thus, although it seems that in samples A and B there are no conditions for a Schottky barrier driven migration of photoholes generated with visible light, surface photoexcitation processes seem to be enough to induce the observed change in water contact angle. A scheme in this sense was proposed by us in a previous publication with N-doped TiO_2 samples prepared by nitrogen implantation where we also explained why the wetting angle does not necessarily yield the superhydrophobic state (i.e., wetting angle lower than 10°).[23]

5. Conclusions

In this paper, we have prepared N-doped TiO_2 thin films by PECVD and GAPVD. We have been able to prepare samples that are amorphous (samples C and E), partially amorphous (samples D), samples with the anatase structure (samples A and B), and other sets of samples (samples F) that consists of a mixture of anatase and rutile. Samples D and particularly E were partially reduced and presented a relative high absorption in the visible ($\lambda = 500$ nm) that is not attributed to the incorporation of nitrogen within their structure.

Different nitrogen species have been detected in the samples by XPS. These species have been tentatively attributed to Ti−N and Ti−N−O species. The first one is the majority in samples D−E and its formation in our films is associated with working conditions that induce a certain reduction of the titanium oxide lattice (i.e., some hydrogen in the plasma or deposition conditions where ion bombardment effects may have a considerable importance). Under partially oxidant conditions as those used for the preparation of samples A, B, and F, Ti−N−O-like species are majority. Samples A and B, both containing relatively low concentration of species Ti−N−O, did not present photocatalytic activity in the visible (i.e., Schottky barrier driven photoactivity) and were less efficient for the photocatalytic degradation of dye solutions under UV irradiation than the reference anatase sample. By contrast, the wetting contact angle on its surface decreased when irradiated with visible light (i.e., these samples presented visible surface photoactivity). This suggests that this kind of nitrogen species is the responsible of the visible photoactivity of N-doped TiO_2. It is also proposed that the wide and sometimes contradictory set of results in the literature relating photoactivity and type of nitrogen species can be the result of the heterogeneous distribution of the Ti−N and Ti−N−O species within the samples, in such a way that active zones or grains with the required type and concentration of nitrogen species are the sole responsible for the visible activity of the whole specimen.

From our samples, only sample F presented both surface and Schottky barrier driven photoactivities in the visible. This sample only had Ti−N−O like species incorporated in its structure but consisted of a mixture of the anatase and rutile phases. This type of sample also presented some absorption features in the visible and a shifted position of the absorption edge. Further theoretical and experimental work is being undertaken to ascertain all the factors that are required for Schottky barrier driven photoactivity with visible light in N-doped TiO_2 systems.

Acknowledgment. We thank the Ministry of Science and Education of Spain (Projects MAT 2007-65764/NAN2004-09317, and the CONSOLIDER INGENIO 2010-CSD2008-00023) and the Junta de Andalucia (Projects TEP2275 and P07-FQM-03298) for financial support. This work has been carried out within the EU project NATAMA (Contract no. 032583).

Supporting Information Available: This material is available free of charge via the Internet at http://pubs.acs.org.

References and Notes

(1) Asahi, R.; Morikawa, T.; Ohwaki, T.; Aoki, K.; Taga, Y. *Science* **2001**, *293*, 269.
(2) Sakthivel, S.; Janczarek, M.; Kirsch, H. *J. Phys. Chem. B* **2004**, *108*, 19384.
(3) Diwald, O.; Thompson, T. L.; Zubkov, T.; Goralski, E. G.; Walck, S. D.; Yates, J. T. *J. Phys. Chem. B* **2004**, *108*, 6004.
(4) Nosaka, Y.; Matsushita, M.; Nasino, J.; Nosaka, A. Y. *Sci. Technol. Adv. Mater.* **2005**, *6*, 143.
(5) Nakano, Y.; Morikawa, T.; Ohwaki, T.; Taga, Y. *Appl. Phys. Lett.* **2005**, *86*, 132104.
(6) Diwald, O.; Thompson, T. L.; Goralski, E. G.; Walck, S. D.; Yates, J. T. *J. Phys. Chem. B* **2004**, *108*, 52.
(7) Yates, H. M.; Nolan, M. G.; Sheel, D. W.; Pemble, M. E. *J. Photochem. Photobiol., A* **2006**, *179*, 223.
(8) Livraghi, S.; Paganini, M. C.; Giamello, E.; Selloni, A.; Valentin, C. D.; Pacchioni, G. *J. Am. Chem. Soc.* **2006**, *128*, 15666.
(9) Lee, J.-Y.; Park, J.; Cho, J.-H. *Appl. Phys. Lett.* **2005**, *87*, 011904.
(10) Thompson, T. L.; Yates, J. T. *Chem. Rev.* **2006**, *106*, 4428.
(11) Emeline, A. V. Kuznetsov, V. N. Rybchuk, V. K. Serpone, N. *Int. J. Photoenergy* **2008**, DOS: 10.1155/2008/258394.
(12) Chen, X.; Burda, C. *J. Phys. Chem.* **2004**, *B108*, 15446.
(13) Sato, S.; Nakamura, R.; Abe, S. *Appl. Catal., A* **2005**, *284*, 131.
(14) Gopinath, C. S. *J. Phys. Chem. B* **2006**, *110*, 7079.
(15) Nakamura, R.; Tanaka, T.; Nakato, Y. *J. Phys. Chem. B* **2004**, *108*, 10617.
(16) Vitiello, R. P.; Macak, J. M.; Ghicov, A.; Tsuchiya, H.; Dick, L. F. P.; Schmuki, P. *Electrochem. Commun.* **2006**, *8*, 544.
(17) Mwabora, J. M.; Lindgren, T.; Avendano, E.; Jaramillo, T. F.; Lu, J.; Lindquist, S. E.; Granqvist, C. G. *J. Phys. Chem. B* **2004**, *108*, 20193.
(18) Irie, H.; Washizuka, S.; Watanabe, Y.; Kako, T.; Hashimoto, K. *J. Electrochem. Soc.* **2005**, *152*, E351.
(19) Yang, M.-Ch.; Yang, T.-S.; Wong, M.-Sh. *Thin Soid Films* **2004**, *469/470*, 1.
(20) Yang, T.-S.; Yang, M.-Ch.; Shiu, Ch.-B.; Chang, W.-K.; Wong, M.-Sh. *Appl. Surf. Sci.* **2006**, *252*, 3729.
(21) Maeda, M.; Watanabe, T. *J. Electrochem. Soc.* **2006**, *153*, C186.
(22) Rico, V. Romero, P. Hueso, J. L. Espinós, J. P. González-Elipe, A. R. *Catal. Today* **2009**, *143*, 347.
(23) Borrás, A.; López, C.; Rico, V.; Gracia, F.; González-Elipe, A. R.; Richter, E.; Battiston, G.; Gerbasi, R.; McSporran, N.; Sauthier, G.; György, E.; Figueras, A. *J. Phys. Chem. C* **2007**, *111*, 1801.
(24) Borrás, A.; Cotrino, J.; González-Elipe, A. R. *J. Electrochem. Soc.* **2007**, *154*, 152.
(25) Gracia, F.; Holgado, J. P.; González-Elipe, A. R. *Langmuir* **2004**, *20*, 1688.
(26) Korzec, D.; Werner, F.; Winter, R.; Engemann, J. *Plasma Sources Sci. Technol.* **1996**, *6*, 216.
(27) van Popta, A. C.; Cheng, J.; Sit, J. C.; Brett, M. J. *J. Appl. Phys.* **2007**, *102*, 013517.
(28) Hawkeye, M. M.; Brett, M. J. *J. Vac. Sci. Technol., A* **2007**, *25*, 1317.
(29) Rico, V. Borrás, A. Yubero, F. Espinós, J. P. Frutos, F. González-Elipe A. R. *J. Phys. Chem. C* **2009**, *113*, 3775.
(30) Dood, J. A.; Lipson, S. J.; Flanagan, D. J.; Blumberg, W. A. M.; Person, J. C.; Green, B. O. *J. Chem. Phys.* **1991**, *94*, 4301.
(31) Ohsaka, T.; Izumi, F.; Fujiki, Y. *J. Raman Spectrosc.* **1978**, *7*, (6).
(32) Zhang, J.; Li, M.; Feng, Z.; Chen, J.; Li, Can *J. Phys. Chem. B* **2006**, *110*, 927.
(33) Cong, Y.; Zhang, J.; Chen, F.; Anpo, M. *J. Phys. Chem. C* **2007**, *111*, 6976.
(34) Kontos, A. I.; Kontos, A. G.; Tsoukleris, D. S.; Vlachos, G. D.; Faralas, P. *Thin Solid Films* **2007**, *515*, 7370.
(35) Kontos, A. I.; Kontos, A. G.; Raptis, Y. S.; Faralas, P. *Phys. Status Solidi* **2008**, *83* (2), 83.
(36) Parker, J. C.; Siegel, R. W. *Appl. Phys. Lett.* **1990**, *57*, 943.
(37) Gyorgy, E.; Pérez del Pino, A.; Serra, P.; Morenza, J. L. *Appl. Surf. Sci.* **2002**, *186*, 130.
(38) Martin, N.; Besnard, A.; Sthal, F.; Vaz, F.; Nouveau, C. *Appl. Phys. Lett.* **2008**, *93*, 064102.
(39) Serpone, N.; Lawless, D.; Khairutdinov, R. *J. Phys. Chem.* **1995**, *99*, 16646.
(40) Vyacheslav, N.; Kuznetsov, N.; Serpone, N. *J. Phys. Chem. B* **2006**, *110*, 25203.
(41) Umebayashi, T.; Yamaki, T.; Itoh, H.; Asai, K. *Appl. Phys. Lett.* **2002**, *81*, 554.
(42) Lei, Z.; Ma, G.; Liu, M.; You, W.; Yan, H.; Wu, G.; Takata, T.; Hara, M.; Domen, K.; Li, C. *J. Catal.* **2006**, *237*, 322.
(43) Liu, B.; Wen, L.; Zhao, X. *Sol. Energy Mater. Sol. Cells* **2008**, *92*, 1.
(44) lin, Z.; Orlov, A.; Lambert, R. M.; Payne, M. C. *J. Phys. Chem. B* **2005**, *109*, 20948.
(45) Bullock, E. L.; Patthey, L.; Steinemann, S. G. *Surf. Sci.* **1996**, *532/534*, 504.
(46) González-Elipe, A. R.; Espinós, J. P.; Fernández, A.; Munuera, G. *Appl. Surf. Sci.* **1990**, *45*, 103.
(47) Leinen, D.; Fernández, A.; Espinós, J. P.; González-Elipe, A. R. *Appl. Phys. A* **1996**, *63*, 237.
(48) Zhao, Y.; Qiu, X.; Burda, C. *J. Phys. Chem.* **2008**, *20*, 2629.
(49) Clouser, S.; Samia, A. C. S.; Navok, E.; Alred, J.; Burda, C. *Top. Catal.* **2008**, *47*, 42.
(50) Qiu, X.; Zhao, Y.; Burda, C. *Adv. Mater.* **2007**, *19*, 3995.

(51) Asahi, R.; Morikawa, T.; Hazama, H.; Matsubara, M. *J. Phys.: Condens. Matter* **2008**, *20*, 064227.
(52) Blochl, P. E. *Phys. Rev. B* **1994**, *50*, 17953.
(53) Lahoz, R.; Espinós, J. P.; de la Fuente, G. F.; González-Elipe, A. R. *Surf. Coat. Technol.* **2008**, *2002*, 1486.
(54) Esaka, F.; Furuya, K.; Shimada, H.; Imamura, M.; Matsubayashi, N.; Sato, H.; Nishijima, A.; Kawana, A.; Ichimura, H.; Kikuchi, T. *J. Vac. Sci. Technol. A* **1997**, *15*, 2521.
(55) Bertoti, I.; Kelly, R.; Mohai, M.; Toth, A. *Surf. Interface Anal.* **1992**, *19*, 291.
(56) Barranco, A.; Holgado, J. P.; Yubero, F.; Espinós, J. P.; Martín, A.; González-Elipe, A. R. *J. Vac. Sci. Technol. A* **2001**, *19*, 1024.
(57) Batich, C. D.; Donald, D. S. *J. Am. Chem. Soc.* **1984**, *106*, 2758.
(58) Zhao, Y.; Qiu, X.; Bruda, C. *Chem. Mater.* **2008**, *20*, 2629.
(59) Okada, M.; Yamada, Y.; Jin, P.; Tazawa, M.; Yoshimura, K. *Appl. Surf. Sci.* **2007**, *254*, 156.
(60) Yang, T.-S.; Yang, M.Ch.; Shiu, Ch.-B.; Chang, W.-K.; Wong, M-Sh. *Appl. Surf. Sci.* **2006**, *252*, 3729.
(61) Yang, M-Ch.; Yang, T.-S.; Wong, M.-Sh. *Thin Sol. Films* **2004**, *469/470*, 1.
(62) Wang, R.; Hashimoto, K.; Fujishima, A.; Chikuni, M.; Kojima, E.; Kitamura, A.; Shimohigoshi, M.; Watanabe, T. *Nature* **1997**, *388*, 431.
(63) Borrás, A.; Barranco, A.; González-Elipe, A. R. *Langmuir* **2008**, *24*, 8021.
(64) Li, Q.; Shang, J.-K. *J. Am. Chem. Soc.* **2008**, *91*, 3167.
(65) Premkumar, J. *Chem. Mater.* **2004**, *16*, 3980.
(66) Carp, O.; Huisman, C. L.; Reller, A. *Prog. Solid State Chem.* **2004**, *32*, 33.
(67) Zhang, J.; Xu, Q.; Feng, Z.; Li, M.; Li, C. *Angew. Chem., Int. Ed.* **2008**, *47*, 1766.

JP9024816